Correlations in sea-level elevations

P. Dimon,[1] J. D. Pietrzak,[2,*] and H. Svensmark[2]
[1]*The Center for Chaos and Turbulence Studies, The Niels Bohr Institute, Blegdamsvej 17, DK-2100 Copenhagen Ø, Denmark*
[2]*Danish Meteorological Institute, Lyngbyvej 100, DK-2100 Copenhagen, Denmark*
(Received 21 March 1997)

We have analyzed a 105-year time record of hourly sea-level elevations for the port of Esbjerg, Denmark. In addition to well-known periodic components, the power spectrum has a low-frequency broadband structure which we interpret as having three regimes behaving approximately as f^0, $f^{-1.2}$, and $f^{-2.4}$ with increasing frequency. We attribute this behavior to driven, damped Kelvin waves. In this context, we present a model which considers the correlation function of a damped wave equation driven by a spatially distributed noise source. We have also studied shorter records at other locations which display similar spectra and compared the coherence functions with the model predictions. [S1063-651X(97)01709-1]

PACS number(s): 05.40.+j, 92.10.Hm, 92.60.Dj

I. INTRODUCTION

We have analyzed a 105-year time record of hourly sea-level elevations from the port of Esbjerg, Denmark taken between 1889 and 1994. The record therefore consists of nearly 10^6 data points, which makes possible the averaging necessary to ascertain the shape of the power spectrum. In addition to well-known periodic components such as tidal peaks, the spectrum has a low-frequency broadband structure which we interpret as having three regimes behaving approximately as f^0, $f^{-1.2}$, and $f^{-2.4}$ with increasing frequency.

Power spectra displaying $1/f$ noise occur in many systems [1,2]. It was the strong suggestion of such behavior in the Esbjerg spectrum that encouraged us to look for a simple model based on a diffusive mechanism, as has often been attempted (without success) for resistors [2]. It is known, for example, that the diffusion equation will produce $1/f$ spectra in all dimensions if it is forced to have white noise at the boundaries [3]. However, this is only true for the spectrum of the spatially averaged field, whereas the sea-level records can certainly be regarded as point measurements. Moreover, it is obvious that at higher frequencies one is simply observing some manifestation of gravity waves which presumably requires some form of wave equation.

We have developed a model that, with certain physical assumptions, may explain the important features of the observed spectrum. In particular, we will argue that the sea-level elevation fluctuations in the North Sea are primarily caused by damped Kelvin waves driven by a spatially distributed white noise source. We can then compute the correlation function for various cases, some of which are relevant for the measured spectra. Other measurements of which we are aware [4,5] probably do not fall into the class of systems described by the model.

The paper is organized as follows. In Sec. II we present spectral measurements of the sea-level elevations at Esbjerg and other locations. In Sec. III we develop the model for the correlation function. In Sec. IV we compare the measured data with the results of the model.

II. SPECTRAL MEASUREMENTS

A. Esbjerg

Esbjerg lies at the east end of the North Sea, one of the most intensely studied seas in the world. Figure 1 shows the location of Esbjerg and the other sites discussed in this work which are in or near the North Sea. The Esbjerg record consists of over 105 years of sea-level elevation measurements $\{y_i\}$ taken at 1-h intervals with a 1-cm resolution. The record was closely examined for any defects. The only problem was sporadic gaps in the data resulting from missing measurements which constituted $\sim 3\%$ of the record.

We performed a simple check for stationarity by tracking the yearly mean and standard deviation as shown in Figs.

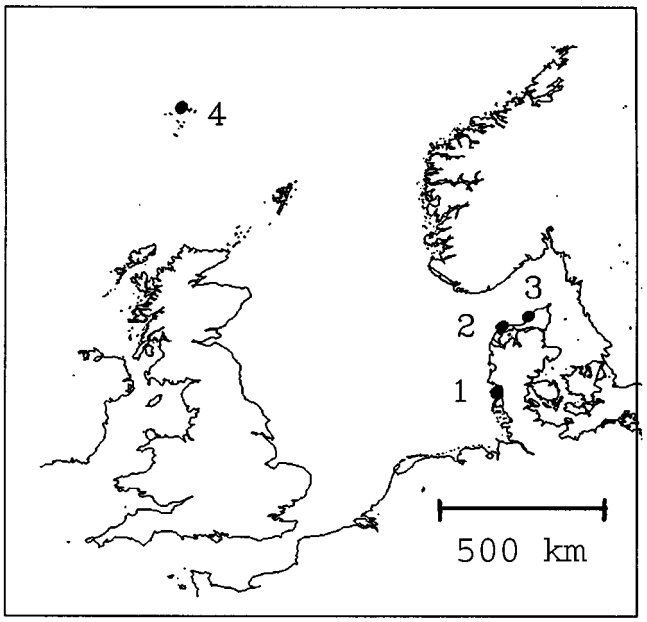

FIG. 1. Map of the North Sea region showing the locations of Esbjerg (1), Hanstholm (2), Hirtshals (3), and Torshavn (4).

*Present address: Danish Hydraulic Institute, Agern Alle 5, DK-2970 Hørsholm, Denmark.

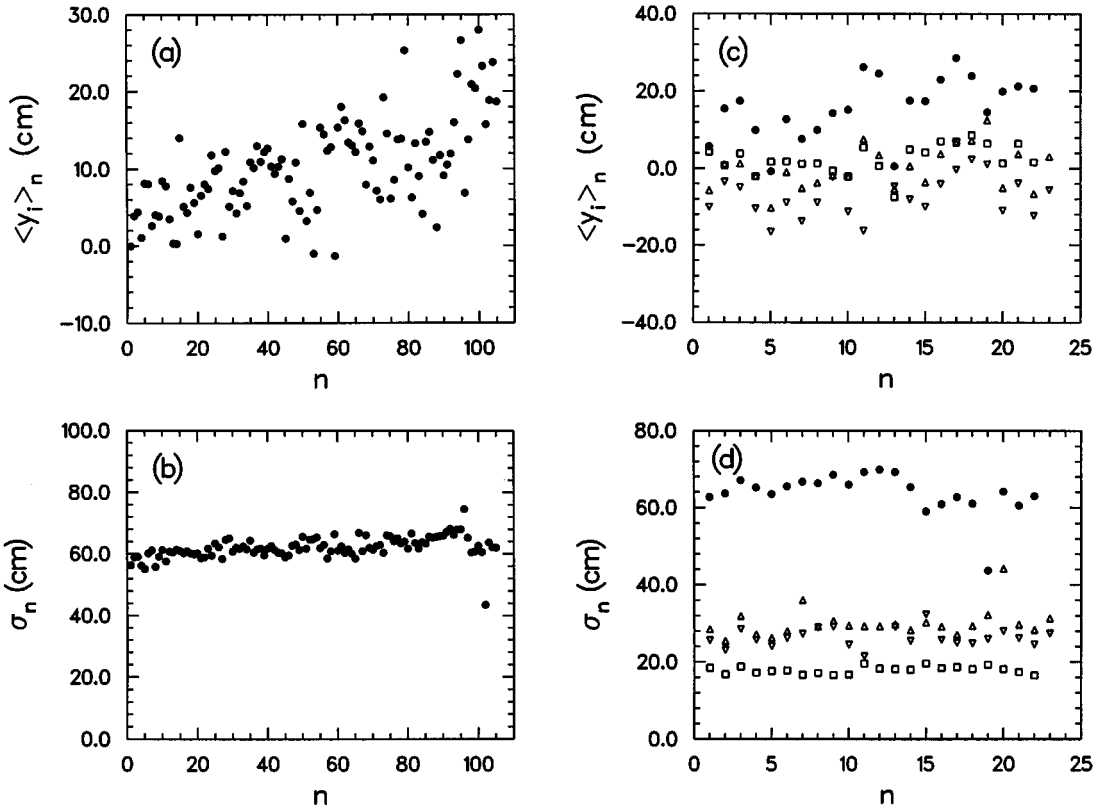

FIG. 2. The nth yearly mean (a) and standard deviation (b) of the Esbjerg data for the period 1889-1994. A similar analysis is shown in (c) and (d) for Esbjerg (●), Torshavn (□), Hanstholm (△), and Hirtshals (▽) for the period 1972–1994. It is evident that Esbjerg has much larger tides than the other sites.

2(a) and 2(b). There is in fact a small, roughly linear increase in time in both the standard deviation ($\sim$10%) and the mean ($\sim$15 cm or $\sim$25% of the standard deviation). Such trends are known to occur [5,6]. They are sufficiently small, however, that if the data are rescaled to have zero mean and a constant standard deviation, the shape of the power spectrum is unaffected. A similar analysis for three other stations in or near the North Sea, albeit with shorter time records ($\sim$22 year), is shown in Figs. 2(c) and 2(d). Both the means and standard deviations appear to be constant over this shorter period of time.

The power spectrum is defined as $S(f)=\langle|\tilde{y}(f)|^2\rangle$, where $\tilde{y}(f)$ is the Fourier transform of the data set $\{y_i\}$, and the angular brackets indicate averaging. In order to compute it, it is necessary to fill in the gaps. This was done by replacing them with the local mean value determined from linear fits through the yearly means shown in Figs. 2(a) and 2(c). Amusingly, the worst gap problems appeared at recent times when the recording apparatus was fully automated. Consequently, in our analysis, we used just the first 720 896 points ($\sim$82 year) which had not only a smaller gap fraction (1.7%) but also far fewer gaps exceeding lengths of 100 which could conceivably contaminate the more interesting lower frequency portion of the spectrum. (As a check, we compared the spectrum for the full data set with the shortened one (both corrected), and found no significant differences, also when the spectra were averaged, implying that the correction alone was sufficient to obtain a clean spectrum. As further evidence that this was the case, we also computed the spectrum of the more gap prone points that were removed, and found it was consistent with the previous spectra. Finally, we computed the spectrum of an essentially gap-free region of the data, and it too was consistent with the others.)

The power spectrum of the Esbjerg data is shown in Fig. 3. Figure 3(a) shows the power spectrum without any averaging. At lower frequencies it is nearly white. At higher frequencies it becomes obscured due to the large statistical fluctuations. To examine higher frequencies, it is therefore necessary to average the power spectrum, and this is the advantage of having such a long time record. This is shown in Fig. 3(b). The length of the averaged segments has been chosen so that the resulting spectrum contains all the essential features of the broadband structure. The crossover to a nearly white spectrum is now seen to occur at $f_\Lambda \sim 5\times10^{-7}$ Hz$\sim$(20 d)$^{-1}$. Above this frequency, there is a region where we believe $S(f)\sim f^{-1.2}$. Then at a frequency $f_c\sim5\times10^{-6}$ Hz$\sim$(2 d)$^{-1}$, the spectrum crosses over rather sharply into a regime where it appears that $S(f)\sim f^{-2.4}$ underneath the tidal peaks. (The spectrum flattens again near the Nyquist frequency, probably as a result of aliasing.) Although we fully realize that this interpretation of the spectrum is open to question, it led us to develop the model discussed in Sec. III, which in turn showed that it is, in fact, a physically plausible possibility.

The lunar tidal peaks are clearly visible at $f\approx1.1\times10^{-5}$ Hz (lunar parallax, 24.84-h period) and $f\approx2.2\times10^{-5}$ Hz (principal lunar, 12.42-h period), plus their various harmonics and sidebands. A blowup of this region is

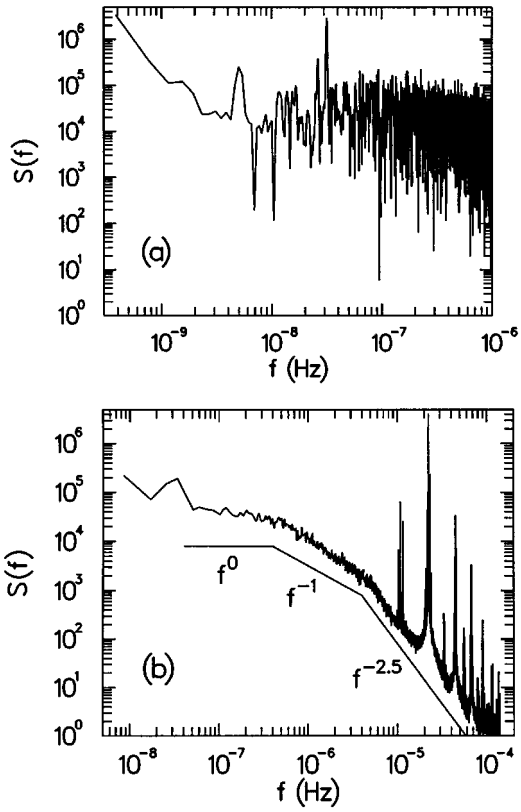

FIG. 3. Power spectrum of the Esbjerg data: (a) Unaveraged. (The first few points reflect the shape of the window function and should be disregarded. Also, the full spectrum up to the Nyquist frequency $f_{\mathrm{Ny}} \simeq 1.4\times10^{-4}$ Hz has not been shown for reasons of clarity.) The solar annual tidal peak can be seen at $f \approx 3.2\times10^{-8}$ Hz. (b) Averaged. The spectrum consists of 46 averages (50% overlap). The lunar tidal peaks are visible at the right. The solid lines are shown for reference.

shown in Fig. 4. Tidal spectra have been studied in great detail, and we will not discuss them further [5,7].

B. Other locations

We have also examined the sea-level elevation records for a number of other sites both in the North Sea and around the globe, a small fraction of which we now present here. Although some of these records cover periods of no more than 25 years, so their spectra cannot be as heavily averaged, they nevertheless yield various clues as to the underlying processes that produce them. Figure 5(a) shows the Esbjerg spectrum from Fig. 3(b) together with the spectrum from Torshavn, Faroe Islands, which lies just at the entrance to the shallow North Sea. Although the Torshavn spectrum consists of only 11 averages, and its broadband structure is therefore less well defined than Esbjerg's, they appear to have roughly the same shape. This also proved to be the case for the ports of Hanstholm and Hirtshals, both of which lie close to Esbjerg on the Danish coast.

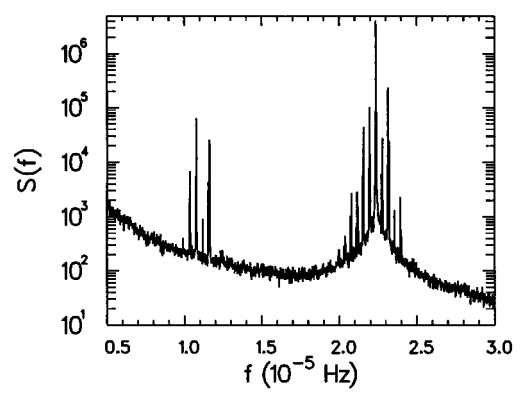

FIG. 4. A blowup of the lunar tidal peaks shown in Fig. 3(b).

This is definitely not the case for locations in other parts of the world. Figure 5(b) compares the spectrum from Esbjerg with one from Hong Kong. The Hong Kong spectrum appears to have the same qualitative behavior as Esbjerg, but both f_Λ and f_c occur at lower frequency. Figures 5(c) and 5(d) show spectra from Antofagasta, Chile and the Yap Islands, respectively, neither of which is even qualitatively similar to Esbjerg's. We will discuss these spectra further in Sec. IV.

C. Spatial correlations

It is also instructive to examine the cross-spectrum $S(\mathbf{x}_1,\mathbf{x}_2,f)=\langle\tilde{y}(\mathbf{x}_1,f)\tilde{y}^*(\mathbf{x}_2,f)\rangle$ between sites at $\mathbf{x}_1$ and $\mathbf{x}_2$ to study spatial correlations. The cross-spectrum can be normalized to form the coherence function $\kappa(f)=S(\mathbf{x}_1,\mathbf{x}_2,f)/\sqrt{S_1(f)S_2(f)}$, so that $|\kappa(f)|$ lies between 0 and 1. The magnitudes of the coherence function for Esbjerg-Torshavn and Hanstholm-Esbjerg are shown in Fig. 6(a). They indicate that the respective pairs of sites are correlated, especially at low frequencies, which is perhaps not surprising. As might be expected, Hanstholm is more correlated with Esbjerg than Torshavn since it is much closer. Of greater interest is the phase of the coherence function $\Theta(f)$ which is shown in Fig. 6(b). In both cases, it increases almost linearly up to $\sim10^{-5}$ Hz, beyond which it can no longer be reliably determined. This suggests that at certain frequencies there is a single characteristic time associated with the flow of information. For dispersion-free waves, this would simply be the transit time between sites, which would explain the larger slope for Esbjerg-Torshavn. Furthermore, the sign of the phase determines the flow direction: Torshavn to Esbjerg to Hanstholm. We will discuss the implications of the phase further in Sec. IV. The coherence function for widely separated sites, such as that for Esbjerg and Hong Kong, shows no signs of correlations except at the tidal peaks.

III. SYSTEM MODEL

We assume that the system is linear, which will be true as long as the wave amplitude A is small compared to the wavelength λ. We will also assume that we are always in the shallow-water limit, i.e., that the unperturbed water depth h is also very small compared to λ. It is well known that, for a constant depth (undamped), shallow-water gravity waves obey the ordinary wave equation $(1/c^2)\partial^2\varphi/\partial^2 t=\nabla^2\varphi$ where $\varphi(\mathbf{x},t)$ is the displacement of the water from its equilibrium height, and $c=\sqrt{gh}$ is the wave velocity where g is the gravitational acceleration [8]. Its dispersion relation is

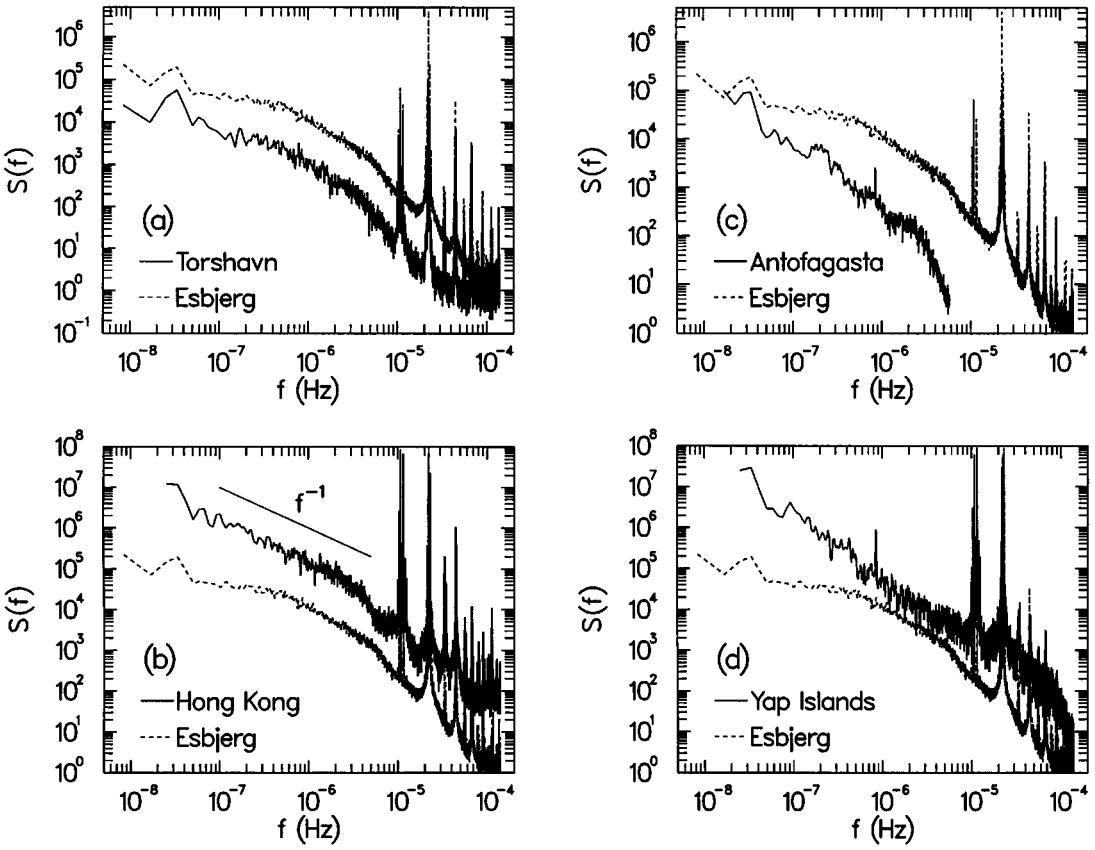

FIG. 5. Comparison of the Esbjerg power spectrum with those of (a) Torshavn, (b) Hong Kong, (c) Antofagasta, Chile, and (d) Yap Islands.

$f=\pm c/\lambda$ (or $\omega=\pm ck$). The linearity condition breaks down at short wavelengths, which for the highest frequencies in Fig. 3(b) ($f\sim 10^{-4}$ Hz) and even a very small water depth $h=10$ m gives $\lambda\sim 10^{5}$ m, whereas generally $A<10$ m. The shallow-water condition requires in addition that $h\ll\lambda$ which is satisfied even in the deepest oceans.

A. Kelvin waves

The rotation of the earth affects the motion of gravity waves, primarily due to the Coriolis force. For example, in a rotating channel of uniform shallow depth in a flat geometry, the equation of motion becomes [8]

$$\frac{\partial}{\partial t}\left(\frac{\partial^2\varphi}{\partial t^2}+\omega_f^2\varphi-c^2\nabla^2\varphi\right)=0, \tag{1}$$

with the boundary conditions

$$\frac{\partial^2\varphi}{\partial y\,\partial t}-\omega_f\frac{\partial\varphi}{\partial x}=0, \quad y=0,L, \tag{2}$$

where (x,y) are the directions along the channel axis and transverse to it, respectively, ω_f is twice the rotation frequency of the channel, and L is its width. We will assume that this simple system describes gravity waves in the North Sea (f-plane approximation). (We regard the depth as constant, on average. We therefore do not consider topographic

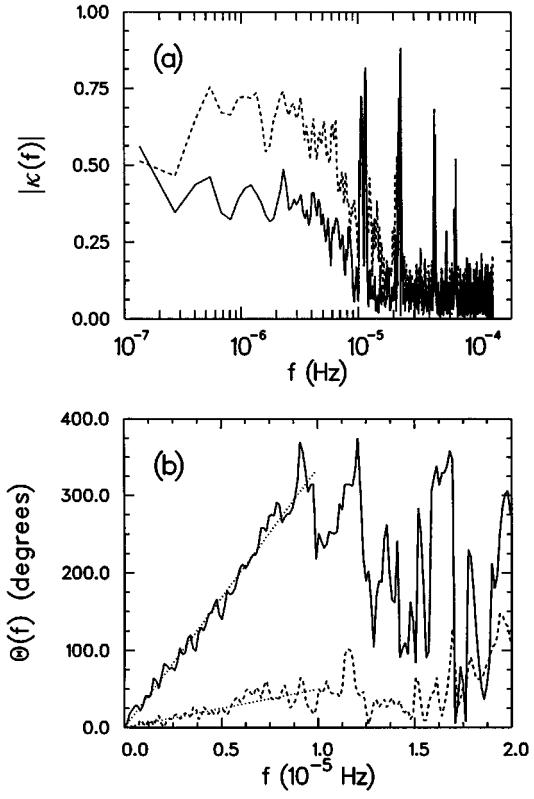

FIG. 6. The magnitude (a) and phase (b) of the coherence function for Esbjerg-Torshavn (solid line) and Hanstholm-Esbjerg (dashed line). The dotted lines in (b) are linear fits (see text).

waves such as Rossby waves. Furthermore, we ignore doppler shifting since even a fast sea current travels no more than ~ 1 m/s.)

This system has two types of propagating waves. The first is Poincaré waves which satisfy the dispersion relation $\omega^2=\omega_f^2+c^2(k^2+n^2\pi^2/L^2)$, where n is an integer. The lowest-lying Poincaré mode in the North Sea, i.e., $n=1$ with $\omega_f=1.2\times10^{-4}$ Hz, $h=100$ m, and $L=500$ km, would be expected to occur at $f\sim3\times10^{-5}$ Hz in the vicinity of the tidal peaks. However, Poincaré waves are generally not observed [9], probably because they are sensitive to the geometry, which is not regular, and hence are effectively smeared out.

The second type is Kelvin waves, which obey the ordinary one-dimensional wave equation along the channel axis and hence have the dispersion relation $\omega=\pm ck$. However, in the transverse direction, they have a time-independent profile $\varphi(y)\sim e^{\mp y/R}$ for waves traveling in the $\pm x$-direction, where $R=c/\omega_f$ is the Rossby radius of deformation. For a water depth $h=100$ m, $c\sim30$ m/s, and $R\sim250$ km. Thus, in the North Sea, Kelvin waves near the coast propagate essentially counterclockwise, since the amplitude of the opposite going waves is diminished by a factor of roughly $1/e^2$. We therefore assume that gravity waves in the North Sea are purely unidirectional Kelvin waves which can be described by the one-dimensional wave equation.

B. Telegraph equation

Next, we must include the effects of damping, i.e., the viscosity ν. It can be shown that in the extreme shallow-water limit $kh\to0$, the dispersion relation for damped gravity waves becomes $\omega=-igk^2h^3/3\nu$, i.e., the motion is purely diffusive with diffusion constant $D_0=gh^3/3\nu$ [10]. Thus, at sufficiently low frequencies gravity waves are overdamped and they conveniently obey the ordinary diffusion equation $\partial\varphi/\partial t=D_0\nabla^2\varphi$. There is one important consideration, however. The Reynold's number of even a rather shallow ($h=100$ m) sea current typical of the North Sea (mean velocity $\overline{v}\sim0.3$ m/s) is $\mathrm{Re}=h\overline{v}/\nu\approx3\times10^7$, so the flow is clearly turbulent. In such a case, the effective viscosity can be much larger. It has been argued that this turbulent viscosity is roughly given by $\nu_t/\nu\sim\mathrm{Re}/\mathrm{Re}_c$ where Re_c is the critical Reynold's number associated with the system [11]. For a sphere, for example, $\mathrm{Re}_c\sim100$, but, for plane Poiseuille flow, it is much larger, in fact $\mathrm{Re}_c\sim6000$, so it is possible that $\nu_t/\nu\sim10^4-10^5$. This is consistent with the estimated vertical turbulent viscosity of the ocean $A_V\sim1-1000$ cm^2/s [8]. (Since turbulent motion only occurs at scales smaller than the water depth, it will not otherwise affect shallow-water gravity waves whose wavelengths, by definition, are much larger.)

The wave and diffusive properties of shallow-water gravity waves can be expressed by the so-called telegraph equation usually used to describe the propagation of electromagnetic waves in a conducting medium,

$$\frac{1}{c^2}\frac{\partial^2\varphi}{\partial t^2}+\gamma\frac{\partial\varphi}{\partial t}-\nabla^2\varphi=F(\mathbf{x},t), \tag{3}$$

where γ is a positive damping constant and $F(\mathbf{x},t)$ is a source term. Its dispersion relation is $D(\mathbf{k},\omega)=k^2-K^2=0$, where $K^2=\omega^2/c^2+i\gamma\omega$. The telegraph equation has the desired limiting behavior with respect to the crossover frequency $\omega_c=\gamma c^2$. At low frequencies $\omega\ll\omega_c$ it reverts to the diffusion equation. We then see that $\gamma=D_0^{-1}$, and consequently $\omega_c=3\nu_t/h^2$. (Following our discussion above, we will henceforth use the turbulent viscosity in place of the ordinary viscosity.) At high frequencies $\omega\gg\omega_c$ it will behave as a wave equation.

The crossover frequency ω_c has a simple physical interpretation, i.e., it is where the penetration depth $\delta=(2\nu_t/\omega)^{1/2}\sim h$. At high frequencies the penetration depth is small, and dissipation at the bottom is not important. At low frequencies the penetration depth becomes comparable to the depth, dissipation becomes dominant, and waves can no longer propagate, i.e., one only observes relaxation. As we will show later, this crossover appears in the power spectrum and it is in fact the same one visible in Fig. 3(b) at $f\sim5\times10^{-6}$ Hz, as discussed in Sec. II A. For a depth $h=100$ m this implies that $\nu_t/\nu\sim10^5$ which is consistent with our rough estimate earlier.

If we write $K=k_0+i\beta$, then, for the telegraph equation,

$$\left.\begin{matrix}k_0\\ \beta\end{matrix}\right\}=\frac{\omega}{c}\left[\frac{\sqrt{1+\omega_c^2/\omega^2}\pm1}{2}\right]^{1/2}. \tag{4}$$

At low frequencies $\beta\simeq(\gamma\omega/2)^{1/2}=(3\nu_t\omega/2gh^3)^{1/2}$. At high frequencies $\beta\to\gamma c/2$, but this cannot be correct since the manner in which γ was introduced was valid only at low frequencies. In fact, for shallow-water gravity waves in the weak-damping approximation it can be shown that [12]

$$\beta\simeq(\nu_t\omega/8gh^3)^{1/2}. \tag{5}$$

For $\nu_t=0.1$ m^2/s and $h=100$ m, this is valid up to $f\sim10^{-2}$ Hz. For reference, the damping length at $f=10^{-4}$ Hz is then $\beta^{-1}\sim1000$ km.

C. Noise source

We now imagine that the Kelvin waves are driven by unspecified random forces. We will therefore use the Langevin approach, and summarize these forces as a stochastic source term. However, their spatial distribution may depend on their origin. For example, the tide in the North Sea enters from the Norwegian Sea and runs counterclockwise with an amphidrome near its center [9,13]. The tide motion is therefore effectively one dimensional (albeit rotating), with an apparent source in the North Atlantic. Since the tides in the North Sea are, in fact, due to Kelvin waves, we may suppose that the Kelvin waves have a local source also, at least at low frequencies. (Local forcing has been considered previously for the diffusion equation, but by employing noisy boundary conditions [3]. However, there are no such apparent boundary conditions in the North Sea, so a source term seems more appropriate.) For a one-dimensional system, the obvious and simplest choice is a point source. At high frequencies, on the other hand, the system is more likely to be driven globally by wind forces or atmospheric pressure variations. In this case the source is translationally invariant in space as well as in time.

A spatially distributed source can be written as $F(\mathbf{x},t)=a(\mathbf{x})\,\eta(\mathbf{x},t)$ where $a(\mathbf{x})$ is the spatial amplitude, and, as usual,

$$\langle \eta(\mathbf{x},t)\rangle = 0, \tag{6a}$$

$$\langle \eta(\mathbf{x},t)\,\eta(\mathbf{x}',t')\rangle = 2\Gamma\,\delta(\mathbf{x}-\mathbf{x}')\,\delta(t-t') \tag{6b}$$

for some constant Γ. For a global (spatially uniform) source $a(\mathbf{x})=1$. For a point source at $\mathbf{x}_0$, $a(\mathbf{x})=\delta(\mathbf{x}-\mathbf{x}_0)$ and the spatial δ function in Eq. (6b) should be replaced with a Kronecker delta. The correlation function of $F(\mathbf{x},t)$ can then be written as

$$\begin{aligned} S_F(\mathbf{x},\mathbf{x}',t,t') &= \langle F(\mathbf{x},t)F(\mathbf{x}',t')\rangle \\ &= 2\Gamma\rho(\mathbf{x})\,\delta(\mathbf{x}-\mathbf{x}')\,\delta(t-t'), \end{aligned} \tag{7}$$

where for a global source $\rho(\mathbf{x})=[a(\mathbf{x})]^2=1$ and for a point source $\rho(\mathbf{x})=\delta(\mathbf{x}-\mathbf{x}_0)$. (Of course, Γ must be different for the two cases.)

In the diffusive limit ($\omega \ll \omega_c$) the noise is nonconserving, i.e., the fluid displacement φ (and hence, for an incompressible fluid, the fluid volume) will not be strictly conserved [14]. In fact, this is desirable since, at low frequencies and hence for long times, one does not expect strict conservation due to nonconserving processes such as rain and evaporation. For short times, however, one expects the water height to be conserved. Although the situation is more complicated in the wave regime ($\omega \gg \omega_c$), the form Eq. (7) can, in fact, be consistent with a conserving source if there are height fluctuations due to noise in the hydrostatic forces, presumably originating from the boundary conditions at the surface. In this case we can just regard the wave equation as the force equation for the surface displacement.

D. Correlation function

We can now compute the correlation function $S(\mathbf{x},\mathbf{x}',t,t')=\langle\varphi(\mathbf{x},t)\varphi(\mathbf{x}',t')\rangle$. Using the Fourier transform $\widetilde{\varphi}(\mathbf{x},\omega)=\int\varphi(\mathbf{x},t)e^{i\omega t}dt$, we first write $\widetilde{\varphi}(\mathbf{x},\omega)=\int\widetilde{G}(\mathbf{x},\mathbf{x}',\omega)\widetilde{F}(\mathbf{x}',\omega)d^dx'$, where $\widetilde{G}(\mathbf{x},\mathbf{x}',\omega)$ is the infinite domain Green's function and d is the dimension of the system. The correlation function can then be written as [15,16]

$$\begin{aligned} S(\mathbf{x}_1,\mathbf{x}_2,\omega) = \int & \widetilde{G}(\mathbf{x}_1,\mathbf{x}',\omega)\widetilde{G}^*(\mathbf{x}_2,\mathbf{x}'',\omega) \\ & \times S_F(\mathbf{x}',\mathbf{x}'',\omega)d^dx'\,d^dx''. \end{aligned} \tag{8}$$

From Eq. (7) we have that $S_F(\mathbf{x},\mathbf{x}',\omega)=2\Gamma\rho(\mathbf{x})\,\delta(\mathbf{x}-\mathbf{x}')$, and so,

$$S_N(\mathbf{x}_1,\mathbf{x}_2,\omega) = \int \widetilde{G}(\mathbf{x}_1,\mathbf{x}',\omega)\widetilde{G}^*(\mathbf{x}_2,\mathbf{x}',\omega)\rho(\mathbf{x}')d^dx', \tag{9}$$

where $S_N(\mathbf{x}_1,\mathbf{x}_2,\omega)=S(\mathbf{x}_1,\mathbf{x}_2,\omega)/2\Gamma$. For a point source at $\mathbf{x}_0$, this simplifies to

$$S_N(\mathbf{x}_1,\mathbf{x}_2,\omega)=\widetilde{G}(\mathbf{x}_1,\mathbf{x}_0,\omega)\widetilde{G}^*(\mathbf{x}_2,\mathbf{x}_0,\omega). \tag{10}$$

The spectral form of the correlation function corresponds, of course, to the cross-spectrum discussed in Sec. II C.

The power spectrum is just the correlation function measured at a single point, i.e., $\mathbf{x}_1=\mathbf{x}_2=\mathbf{x}$. For a global source [$\rho(\mathbf{x})=1$] this is,

$$S_N(\omega)=\int|\widetilde{G}(\mathbf{x},\mathbf{x}',\omega)|^2d^dx'. \tag{11}$$

(The system is translationally invariant so the power spectrum must be independent of the measuring position.) For a point source we have,

$$S_N(\mathbf{x},\omega)=|\widetilde{G}(\mathbf{x},\mathbf{x}_0,\omega)|^2. \tag{12}$$

The telegraph equation Eq. (3) has plane-wave eigenfunctions so its Green's function can be written as

$$\widetilde{G}_0(\mathbf{x},\mathbf{x}',\omega)=\frac{1}{(2\pi)^d}\int\frac{e^{i\mathbf{k}\cdot(\mathbf{x}-\mathbf{x}')}}{D(\mathbf{k},\omega)}d^dk, \tag{13}$$

which, for a single source of spatially decaying outgoing waves, is [17]

$$\widetilde{G}_0(x,x',\omega)=(i/2K)e^{iK|x-x'|}\quad(d=1), \tag{14a}$$

$$\widetilde{G}_0(\mathbf{x},\mathbf{x}',\omega)=(i/4)H_0^{(1)}(K|\mathbf{x}-\mathbf{x}'|)\quad(d=2), \tag{14b}$$

$$\widetilde{G}_0(\mathbf{x},\mathbf{x}',\omega)=(1/4\pi|\mathbf{x}-\mathbf{x}'|)e^{iK|\mathbf{x}-\mathbf{x}'|}\quad(d=3), \tag{14c}$$

where $H_0^{(1)}(z)$ is a Hankel function of the first kind and $K=+(\omega^2/c^2+i\gamma\omega)^{1/2}$.

We have not, as yet, discussed the white noise at very low frequencies found in most of the measured spectra. This is presumably a consequence of the finite size Λ of the system, which we have not considered in the analysis so far. This would introduce a cutoff at small wave vectors $k_\Lambda\sim1/\Lambda$ in the integral Eq. (13) with the result that $\widetilde{G}_0(\mathbf{x},\mathbf{x}',\omega)\to$const. when $\omega<\omega(k_\Lambda)$. Hence the correlation function will also become constant below $\omega_\Lambda=\omega(k_\Lambda)$.

It is now straightforward to compute the correlation function explicitly for specific cases. We will consider $d=2$ for completeness, although we have assumed all along that the relevant phenomenon is one-dimensional Kelvin waves.

1. Point source

(a) $d=1$: If both $x_1>x_0$ and $x_2>x_0$, i.e., both measuring points are on the same side of the source, then, substituting Eq. (14a) into Eq. (10) we find,

$$S_N(x_1,x_2,\omega)=\frac{1}{4|K|^2}e^{ik_0\xi}e^{-\beta(x_1-x_0)}e^{-\beta(x_2-x_0)}, \tag{15}$$

where $\xi=x_1-x_2$. The phase is independent of the source position x_0 and is simply

$$\Theta(\omega)=k_0\xi, \tag{16}$$

where $k_0(\omega)$ is given by Eq. (4). We can write the power spectrum Eq. (12) as

$$S_N(x,\omega)=\frac{e^{-2\beta(x-x_0)}}{4\gamma\omega[1+\omega^2/\omega_c^2]^{1/2}}. \tag{17}$$

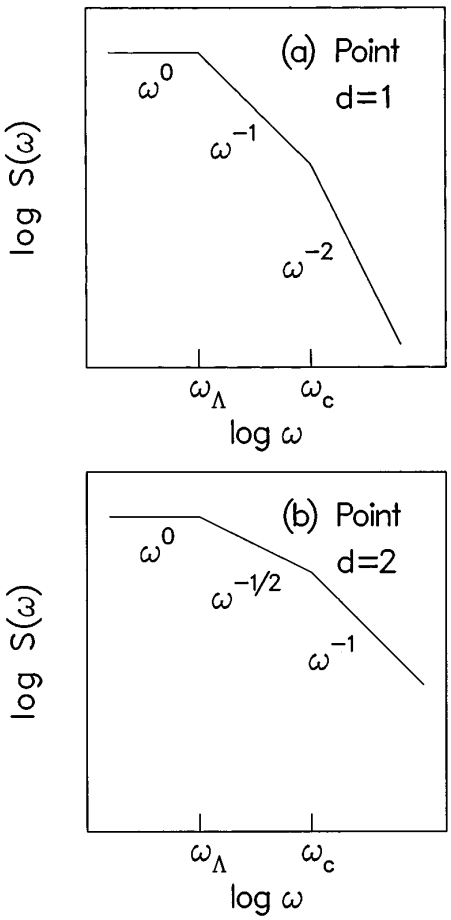

FIG. 7. Power spectra of the telegraph equation driven by a point noise souce for (a) $d=1$ and (b) $d=2$.

It should be noted that β, whose behavior is incorrect at high frequencies as discussed in Sec. III B, only appears in the damping factor. (The phase does not depend on β at all.) Ignoring the damping factor, we see immediately that $S_N(x,\omega)\sim(\gamma\omega)^{-1}$ for $\omega\ll\omega_c$ and $S_N(x,\omega)\sim(\omega/c)^{-2}$ for $\omega\gg\omega_c$.

(b) $d=2$: In this case the correlation function is just

$$S_N(\mathbf{x}_1,\mathbf{x}_2,\omega)=\tfrac{1}{16}H_0^{(1)}(K|\mathbf{x}_1-\mathbf{x}_0|)H_0^{(2)}(K^*|\mathbf{x}_2-\mathbf{x}_0|), \tag{18}$$

and the power spectrum is therefore

$$S_N(\mathbf{x},\omega)=\tfrac{1}{16}|H_0^{(1)}(K|\mathbf{x}-\mathbf{x}_0|)|^2. \tag{19}$$

It is more instructive to use the asymptotic form of the Hankel function $H_0^{(1)}(z)\simeq(2/\pi z)^{1/2}e^{i(z-\pi/4)}$. (We ignore the logarithmic singularity as $z\to 0$, since it can only be observed at frequencies corresponding to length scales far greater than any in the system.) Then Eq. (19) can be written as

$$S_N(\mathbf{x},\omega)\simeq\frac{e^{-2\beta|\mathbf{x}-\mathbf{x}_0|}}{8\pi|K||\mathbf{x}-\mathbf{x}_0|}. \tag{20}$$

The above results are shown schematically in Fig. 7. In general, we find for a point source that (without damping factors)

$$S_N(\mathbf{x},\omega)\sim|K|^{d-3}\sim\begin{cases}\omega^{(d-3)/2} & (\omega\ll\omega_c)\\ \omega^{d-3} & (\omega\gg\omega_c).\end{cases} \tag{21}$$

2. Global source

Using the representation Eq. (13), the correlation function Eq. (9) can be written as

$$S_N(\mathbf{x}_1,\mathbf{x}_2,\omega)=\frac{1}{(2\pi)^d}\int\frac{e^{i\mathbf{k}\cdot(\mathbf{x}_1-\mathbf{x}_2)}}{|D(\mathbf{k},\omega)|^2}d^dk. \tag{22}$$

For an isotropic system $D(\mathbf{k},\omega)$ can only depend on k^2, so the correlation function must be real and hence $\Theta(\omega)=0$ always. A simple scaling of Eq. (22) shows that in the diffusive regime of the telegraph equation ($\omega\ll\omega_c$), the power spectrum behaves as $S_N(\omega)\sim\omega^{(d/2)-2}$. The wave regime behavior is more complicated, and will be discussed shortly.

If, in addition to being isotropic, $\mathrm{Im}D(\mathbf{k},\omega)$ is independent of k, then there is a simple connection between Eqs. (13) and (22), namely,

$$S_N(\mathbf{x}_1,\mathbf{x}_2,\omega)=-\mathrm{Im}\tilde{G}_0(\mathbf{x}_1,\mathbf{x}_2,\omega)/\mathrm{Im}D(\mathbf{k},\omega) \tag{23}$$

which resembles the fluctuation-dissipation theorem [18]. For the special case $D(\mathbf{k},\omega)=k^2-K^2$, this becomes

$$S_N(\mathbf{x}_1,\mathbf{x}_2,\omega)=\mathrm{Im}\tilde{G}_0(\mathbf{x}_1,\mathbf{x}_2,\omega)/2\beta k_0. \tag{24}$$

For the telegraph equation, the infinite domain Green's function is equivalent to the response function, and $2\beta k_0=\gamma\omega$ from Eq. (4), so we recover the fluctuation-dissipation theorem explicitly. As we have discussed, however, β does not behave as predicted by the telegraph equation at high frequencies. This is especially relevant for a global source, since damping is necessary in the wave regime to preserve stationarity (whereas for a point source the energy can radiate away). In principle, the true response function must be computed from the full (linearized) Navier-Stokes equations with the appropriate boundary conditions (from which the true form of β is actually derived), and this is not equivalent to the infinite domain Green's function. Consequently, the form $D(\mathbf{k},\omega)=k^2-K^2$ can no longer be valid for all wave vectors. Nevertheless, it should still correctly describe the high- and low-frequency limiting behavior. Thus, if we use the true form of β in the Green's functions Eqs. (14), they will also retain the correct high- and low-frequency limiting behavior, and thus become useful approximations. [These remarks are also relevant for a point source since β still appears in the damping factors in Eq. (15).]

(a) $d=1$: Using Eq. (14a) and the relation Eq. (24), we find

$$S_N(x_1,x_2,\omega)=\frac{e^{-\beta|\xi|}}{4\beta k_0|K|^2}[k_0\cos(k_0\xi)-\beta\,\sin(k_0|\xi|)]. \tag{25}$$

As expected, the correlation function is real and so the phase is always zero. It also has oscillations that would be observable. The power spectrum ($\xi=0$) is then just

$$S_N(\omega)=1/4\beta|K|^2. \tag{26}$$

This result implicitly assumes that one is measuring waves traveling in both directions. As discussed in Sec. III A, however, Kelvin waves are effectively uni-directional. Thus we must return to Eq. (9) and compute the correlation function by explicitly writing the Green's function Eq. (14a) as a sum of positive- and negative-going waves, i.e.,

$$\tilde{G}_0(x,x',\omega)=(i/2K)[e^{iK(x-x')}\theta(x-x') + e^{-iK(x-x')}\theta(x'-x)], \quad (27)$$

where $\theta(x)$ is the unit step function. Then keeping only the positive-going contribution, Eq. (9) yields

$$S_N(x_1,x_2,\omega)=\frac{1}{8\beta|K|^2}e^{ik_0\xi}e^{-\beta|\xi|}, \quad (28)$$

which has a nonzero phase $\Theta(\omega)=k_0\xi$ just as for a point source. The power spectrum is, of course, just half of what it was for the bidirectional result Eq. (26).

(b) $d=2$: Using Eq. (24) again, we find

$$S_N(\mathbf{x}_1,\mathbf{x}_2,\omega)=\frac{1}{16\beta k_0}[H_0^{(1)}(Kr)+H_0^{(2)}(K^*r)], \quad (29)$$

where $r=|\mathbf{x}_1-\mathbf{x}_2|$. The power spectrum is therefore

$$S_N(\omega)=1/8\beta k_0. \quad (30)$$

The results for a global source are shown schematically in Fig. 8. In general, we find that (ignoring damping factors)

$$S_N(\omega)\sim\beta^{-1}k_0^{d-3}\sim\begin{cases}\omega^{(d/2)-2} & (\omega\ll\omega_c)\\ \omega^{d-3} & (\omega\gg\omega_c).\end{cases} \quad (31)$$

The high-frequency behavior now depends explicitly on β, which it did not for a point source (excluding damping factors). As discussed earlier in this section, we can obtain the correct spectra for damped gravity waves by using the true form of β in Eq. (31). In particular, if we use the weak-damping approximation Eq. (5), then $S_N(\omega)\sim\omega^{d-7/2}$ in the wave regime ($\omega\gg\omega_c$). The corrected spectra are shown as dashed lines in Fig. 8.

3. Power spectrum of the spatially averaged field

The results of the previous sections should also be compared with the spectrum of the spatially averaged field usually presented in the literature [3]. This can be written as $\overline{S_N(\omega)}=\Lambda^{-2d}\int S_N(\mathbf{x}_1,\mathbf{x}_2,\omega)d^dx_1d^dx_2$. Using Eq. (22) we obtain the expected result for a global source $\overline{S_N(\omega)}=\Lambda^{-d}|D(\boldsymbol{k}=\mathbf{0},\omega|^{-2}$. (The result is the same for a point source except that it should be divided by another factor of Λ^d.) In the diffusive regime, we therefore obtain the well-known result $\overline{S_N(\omega)}\sim\omega^{-2}$ which holds in all dimensions. If, on the other hand, the system is forced to have noisy boundaries, as opposed to a noisy source term, then $\overline{S_N(\omega)}\sim\omega^{-1}$ in all dimensions [3]. However, as in the present work, the spatially averaged field is often not what is actually measured.

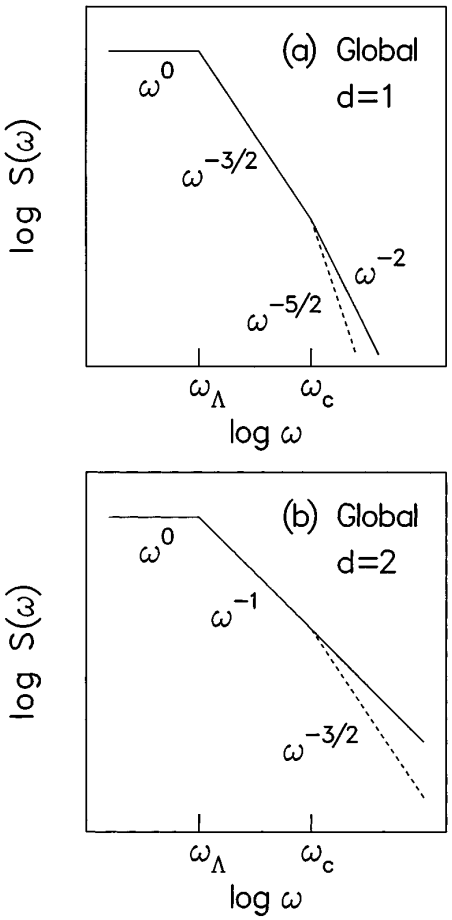

FIG. 8. Power spectra of the telegraph equation driven by a global noise source for (a) $d=1$ and (b) $d=2$. The dashed lines show the corrected spectra using the weak-damping approximation for β [Eq. (5)] (see text).

IV. COMPARISON OF MODEL AND DATA

We will now discuss which of the possible scenarios presented in Sec. III D are relevant for the sea-level elevation data. (We only consider $d=1$, since this was one of the original assumptions of the model.)

A. Damping factor

The damping factors which we have ignored thus far may be important at high frequencies. Using the weak-damping approximation for β, Eq. (5), we can rewrite the damping factor in Eq. (17) as $\exp[-2\beta(x-x_0)]=\exp[-(f/f_0)^{1/2}]$, where $f_0=gh^3/\pi\nu_t(x-x_0)^2$. If $f_0>f_c$, then $x-x_0<(3/2)^{1/2}(c/\pi f_c)\sim 2300$ km. In other words, the fact that we do not see an obvious exponential decay in the Esbjerg spectrum [Fig. 3(b)] implies that the apparent source cannot be further away than this distance. (The stretched exponential dependence of the damping on frequency weakens its effect even more.) Furthermore, as discussed in Sec. II B, we do not observe any significant difference between the Esbjerg and Torshavn spectra. According to the above argument, the latter ought to be much closer to the source, and thus not display any of the effects of damping, if present. We therefore conclude that the damping factors are not important at the studied frequencies.

B. Esbjerg

The Esbjerg spectrum, Fig. 3(b), could perhaps be produced by a point source as given by Eq. (17). From the argument in the previous section, it would have to be located no more than ~ 2000 km away, otherwise the effects of damping would be manifest. This would explain the nonzero phase in the measured cross-spectra with Torshavn and Hanstholm [see Fig. 6(b)] predicted by Eq. (16) (at least in the wave regime, since it is quite impossible to resolve the very small phases in the diffusive regime). However, the measured slopes in the spectrum are noticeably steeper than the predicted ones. It would seem more likely, therefore, based on the arguments of Sec. III C, that the system is driven by global forces, at least in the wave regime where the measured and predicted exponents would then be roughly in agreement. The diffusive regime could still be produced by a point source, although perhaps contaminated by global forcing. A nonzero phase then requires that only unidirectional waves be present as we expect for Kelvin waves in the North Sea.

If we fit the measured phases to the high frequency form of Eq. (16) $\Theta(\omega) \simeq \omega\xi/c$, then for $c = 30$ m/s, we find $\xi \approx 2800$ km for Esbjerg-Torshavn and $\xi \approx 400$ km for Hanstholm-Esbjerg. The first should be compared not with the direct distance between Torshavn and Esbjerg (~ 1200 km), but with the length of the counterclockwise tidal path in the North Sea that the Kelvin waves also presumably follow (~ 2000 km). The second distance is in reality ~ 200 km. The discrepancies may suggest that we have overestimated the wave speed, and hence, the depth, particularly in the relatively shallower water between Esbjerg and Hanstholm.

We can estimate Λ from the crossover to white noise f_Λ in the Esbjerg, spectrum, Fig. 3(b). (The spectrum below f_Λ is actually not quite white which may indicate that the source spectrum may also not be white as we have assumed.) In the diffusive regime $2\pi f_\Lambda \sim D_0 k_\Lambda^2$, which gives $\Lambda = (c/2\pi) \times (f_c f_\Lambda)^{-1/2} \sim 3000$ km. This is roughly the size of the North Atlantic basin.

C. Other locations

The discussion in Sec. IV B also applies to the Hong Kong spectrum Fig. 5(b). As discussed in Sec. II B both f_Λ and f_c occur at lower frequencies than in the Esbjerg spectrum, although the two spectra are otherwise rather similar. The first shift implies that the ''size'' of the Hong Kong system is larger than Esbjerg's. The size might be the length of the continental shelf from the Yellow Sea to the Golf of Tonkin (~ 3000 km). The second implies that ν_t/h^2 is smaller than in the North Sea, but this is difficult to check independently.

The spectrum from Antofagasta, Chile, shown in Fig. 5(c), is probably a consequence of a different process altogether. First, the water is much deeper than in the North Sea ($h > 3000$ m) which should result in a distinctly smaller crossover frequency f_c (bearing in mind that ν_t also depends on h). The measured spectrum would therefore be entirely in the wave regime, but the slope is not consistent with those predicted by our model for either a point or a global source. Second, the Kelvin wave theory requires a uniform depth which is not the case here. In fact, if allowance is made for both the sloping topography at the coast and a realistic density stratification, then it is known that coastal trapped waves can exist causing coastal sea-level fluctuations with time scales of $\sim 1-20$ d [19]. These may be responsible for the observed spectrum. The Yap Islands are in the open sea, so presumably the gravity waves there are not Kelvin waves, and consequently the spectrum Fig. 5(d) cannot be understood in the context of this work.

D. Concluding remarks

It is difficult, of course, to assign a definite explanation to any given spectrum. Unlike a laboratory experiment, it is impossible to make a systematic survey of the various control parameters governing sea-level elevations, or even to obtain the data quality required to resolve competing theories. However, we feel that there is a certain self-consistency between the data and the model presented in this work that is not accidental. Unfortunately, the more interesting spectra where both the diffusive and wave regimes are manifest require rather special conditions, specifically, a large bounded body of relatively shallow water. Nevertheless, the methods employed are sufficiently general that they may be applicable to other systems as well.

ACKNOWLEDGMENTS

It is a pleasure to thank S. C. Creagh and G. Grinstein for many informative discussions.

[1] W. H. Press, Comm. Ast. **7**, 103 (1978).
[2] P. Dutta and P. M. Horn, Rev. Mod. Phys. **53**, 497 (1981); M. B. Weissman, *ibid.* **60**, 537 (1988).
[3] S. H. Liu, Phys. Rev. B **16**, 4218 (1977); K. M. van Vliet, A. van der Ziel, and R. R. Schmidt, J. Appl. Phys. **51**, 2947 (1980); S. C. Miller, Phys. Rev. B **24**, 3008 (1981); H. J. Jensen, Phys. Scr. **43**, 593 (1991); G. Grinstein, T. Hwa, and H. J. Jensen, Phys. Rev. A **45**, R559 (1992).
[4] C. Wunsch, Rev. Geophys. **10**, 1 (1972). More recently, satellite observations have been used to reconstruct global sea-level wavevector distributions: C. Wunsch and D. Stammer, J. Geophys. Res. **100**, 24 895 (1995).
[5] See D. T. Pugh, *Tides, Surges and Mean Sea-Level* (Wiley, New York, 1987).
[6] V. S. Gornitz, S. Lebedeff, and J. Hansen, Science **215**, 1611 (1982).
[7] D. E. Cartwright and A. C. Edden, J. R. Astron. Soc. Can. **33**, 253 (1973).
[8] See, for example, J. Pedlosky, *Geophysical Fluid Dynamics* (Springer-Verlag, New York, 1987).
[9] See, for example, A. E. Gill, *Atmosphere-Ocean Dynamics* (Academic, New York, 1982).
[10] P. H. LeBlond and F. Mainardi, Acta Mech. **68**, 203 (1987); see also Ref. [16], Appendix B.

[11] L. D. Landau and E. M. Lifshitz, *Fluid Mechanics* (Pergamon, Oxford, 1987).

[12] J. N. Hunt, Houille Blanche **19**, 685 (1964). See also L. Montefusco, Rend. Acc. Naz. Lincei **46**, 704 (1969), Ref. [10], and Ref. [16], Appendix B.

[13] M. J. Howarth and D. T. Pugh, in *Physical Oceanography of Coastal and Shelf Seas*, edited by B. Johns (Elsevier, Amsterdam, 1983).

[14] See, for example, T. Hwa and M. Kardar, Phys. Rev. Lett. **62**, 1813 (1989). For strict conservation, one would require that $\langle F(\mathbf{x},t)F(\mathbf{x}',t')\rangle = -2\bar{\Gamma}\boldsymbol{\nabla}\cdot\boldsymbol{\nabla}' a(\mathbf{x})a(\mathbf{x}')\delta(\mathbf{x}-\mathbf{x}')\delta(t-t')$ for some constant $\bar{\Gamma}$.

[15] S. C. Creagh and P. Dimon, Phys. Rev. E **55**, 5551 (1997). A similar expression was obtained earlier by K. M. van Vliet, A. van der Ziel, and R. R. Schmidt in Ref. [3].

[16] S. H. Hansen, S. Hørlück, D. Zauner, P. Dimon, C. Ellegaard, and S. C. Creagh, Phys. Rev. E **55**, 7048 (1997).

[17] See, for example, P. M. Morse and H. Feshbach, *Methods of Theoretical Physics* (McGraw-Hill, New York, 1953).

[18] H. B. Callen and T. A. Welton, Phys. Rev. **83**, 34 (1951); see, for example, D. Forster, *Hydrodynamic Fluctuations, Broken Symmetry, and Correlation Functions* (Benjamin/Cummings, Reading, 1975).

[19] J. M. Huthnance, L. A. Mysak, and D. P. Wang edited by CAGV, Coastal Estuarine Sci. **3**, 1 (1986); K. H. Brink, Annu. Rev. Fluid Mech. **23**, 389 (1991); J. M. Huthnance, Prog. Oceanogr. **35**, 353 (1995).